Research Square

Preprints are preliminary reports that have not undergone peer review.
They should not be considered conclusive, used to inform clinical practice,
or referenced by the media as validated information.

Superpotential enhanced superconductivity and robust stiffness shaped by quantum geometry

Floriana Lombardi

floriana.lombardi@chalmers.se

Chalmers University of Technology, Göteborg, Sweden https://orcid.org/0000-0002-3478-3766

Thilo Bauch

Chalmers University of Technology https://orcid.org/0000-0002-8918-4293

Goetz Seibold

BTU Cottbus-Senftenberg https://orcid.org/0000-0002-1772-1563

Article

Keywords:

Posted Date: January 12th, 2026

DOI: https://doi.org/10.21203/rs.3.rs-8196129/v1

License: This work is licensed under a Creative Commons Attribution 4.0 International License.
Read Full License

Additional Declarations: There is **NO** Competing Interest.

Version of Record: A version of this preprint was published at Communications Physics on October 2nd, 2026. See the published version at https://doi.org/10.1038/s42005-026-02905-z.

Superpotential enhanced superconductivity and robust stiffness shaped by quantum geometry

T. Bauch,[1] F. Lombardi,[1] and G. Seibold[2]

[1] *Quantum Device Physics Laboratory, Department of Microtechnology and Nanoscience, Chalmers University of Technology, SE-41296 Göteborg, Sweden*

[2] *Institut für Physik, BTU Cottbus-Senftenberg, D-03013 Cottbus, Germany*

Enhancing superconductivity through material design is a central goal in quantum materials research. Moiré engineering, where twisting stacked layers creates long-wavelength modulations and flat bands, has shown how electronic correlations can be amplified and eventually used to raise the superconducting critical temperature T_c. Yet this approach is largely confined to van der Waals materials and offers limited tunability. Here we explore a moiré-inspired alternative: imposing artificial superpotentials on otherwise homogeneous systems to engineer flat electronic minibands. Whether such superlattice potentials can truly enhance superconductivity and sustain a finite superfluid stiffness remains, however, an open question. Our calculations show that a periodic superpotential imposed to a 2D system can indeed enhance superconductivity by reconstructing the electronic bands and creating regions of large density of states, leading to a substantial increase of T_c. In contrast to conventional flat band systems, where the superfluid stiffness arises solely from quantum geometry through the quantum metric, a modulated system inherits kinetic energy from the filled minibands below the Fermi level. This inherited component coexists with a positive quantum geometric contribution, yielding a finite and robust stiffness even when the upper band becomes nearly flat. The resulting superconducting state remains coherent and resilient against weak to moderate disorder. Our findings demonstrate that engineered superpotentials offer a tunable route to enhance superconductivity beyond twist based moiré systems, unifying flat band amplification of pairing with preserved phase stiffness. They further highlight the central role of quantum geometry in shaping collective electronic phenomena and point to superlattice design as a promising platform for next-generation superconductors.

When the magic-angle condition in twisted graphene was predicted [1], it opened an unexpected path in condensed matter physics. A subtle geometric twist between two layers produced electronic flat bands and, remarkably, superconductivity [2–9] in a system where electrons were thought to be almost immobile. This discovery triggered an intense theoretical effort to understand how superconductivity could arise when the effective mass is infinite and the conventional contribution to the superfluid weight—linked to carrier motion—vanishes. The key to this puzzle emerged from the quantum geometry concept. It was realized that in flat bands the superfluid stiffness can receive a finite contribution from the quantum metric [10–16], a geometric property of the Bloch wavefunctions, rather than from the band dispersion itself. This insight transformed our understanding of superconductivity, revealing that the wavefunction's geometry, not just its energy, determines the ability of the condensate to support supercurrents.

Today, the concept of quantum geometry extends far beyond moiré materials and plays a fundamental role in a variety of condensed-matter phenomena [17, 18]. For example it has emerged as a key ingredient in systems with non-trivial topology [10, 19, 20], in multiband superconductors [21, 22], and in oxide interfaces such as $LaAlO_3/SrTiO_3$ [23] where a finite quantum metric is associated with spin–momentum locking which provides a tangible example of how real materials can harness geometric effects. Moreover, the quantum geometry of the electronic states can also influence the strength of the interactions like the electron–phonon coupling: bands with a larger quantum metric exhibit enhanced coupling to lattice vibrations [24] which may in turn boost superconductivity. Indeed, flat bands themselves offer a tantalizing prospect: theory predicts that the superconducting transition temperature T_c can scale linearly with the pairing strength U, rather than being exponentially suppressed as in the BCS limit [25–28]. This opens a route to dramatically enhanced superconductivity, potentially even at ambient conditions, if the right quantum geometry is engineered. But must one always rely on twisting between 2D layers to achieve flat bands? While twisting is confined to van der Waals materials, the underlying idea of a moiré-like superpotential could, in principle, be engineered in a much broader class of superconductors.

When a conventional single band superconductor is subject to a periodic superpotential, the folded reduced Brillouin zone hosts minibands that can flatten at sufficiently high potential strength. In this regime, a key question arises: can the essential ingredients of a moiré-based superconductivity—enhanced density of states, elevated T_c, and finite superfluid stiffness—also emerge

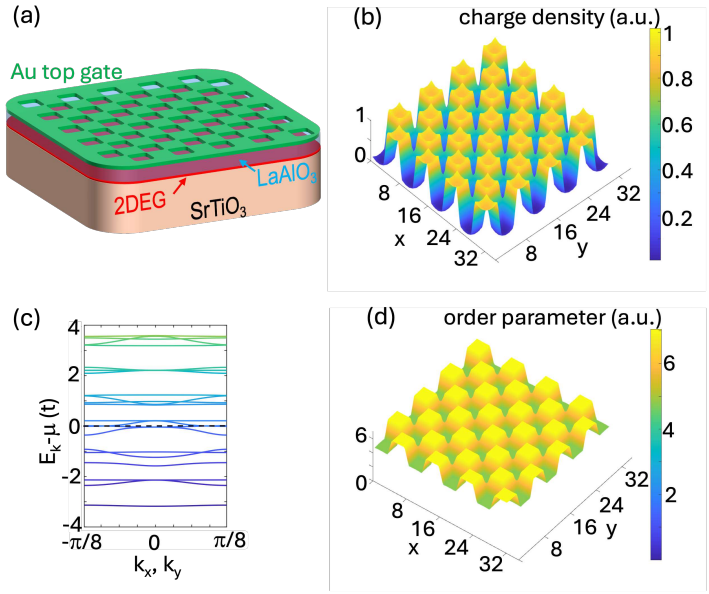


FIG. 1. **Realization and electronic properties of a device with periodidic gating.** (a) Schematic of a 2D superconducting electron gas modulated by a periodic gate potential. A representative platform for realizing such a system is the $LaAlO_3/SrTiO_3$ interface. (b) Color surface plot of the modulated charge density for a checkerboard lattice of 4×4 plaquettes. (c) Band structure for a diagonal cut across the reduced Brillouin zone. (d) Color surface plot of the modulated order parameter. Parameters: $U/t = 1.5$, $V_0/t = 4(c)$, $V_0/t = 2$ (b,d), charge concentration $p = 0.5$.

without geometric twisting?

Traditionally, a superpotential has been viewed as a weak perturbation, incapable of dramatically reshaping the electronic structure or inducing strong-coupling effects. Even when flat bands form at large superpotential amplitudes at the Fermi energy E_F, they are typically not isolated, unlike in twisted graphene at the magic angle, but the remaining folded (and eventually dispersive) bands below E_F still contribute to the response of the system. As a result, it has remained unclear whether band folding alone, i.e. in the absence of the geometric effects of twisting, can produce flat-band physics and superconductivity enhancement.

Here, we demonstrate that contrary to this conventional view, a sufficiently strong superpotential, can indeed generate a flat-band system with a markedly enhanced superconducting transition temperature, T_c. Probing the superfluid stiffness reveals that, while quantum geometry crucially contributes, its dominant component arises from the residual band dispersion of the occupied states below the Fermi level. Thus, even when the band at the Fermi energy becomes flat, the total kinetic energy remains finite, inherited from lower minibands. This mechanism—absent in twisted moiré systems—establishes a new route to robust superconductivity in superpotential-driven flat-band materials and can readily be tested in two-dimensional superconductors as illustrated in Fig. 1a.

ELECTRONIC MULTIBAND STRUCTURE AND CRITICAL TEMPERATURE

Our calculations are based on the following tight-binding hamiltonian

$$H = -t \sum_{\langle ij\rangle,\sigma} c^\dagger_{i,\sigma} c_{j,\sigma} + \sum_{i\sigma} (V_i - \mu)\, n_{i\sigma} - |U| \sum_n \left[n_{n,\uparrow} - \langle n_{n,\uparrow}\rangle\right]\left[n_{n,\downarrow} - \langle n_{n,\downarrow}\rangle\right] , \qquad (1)$$

which contains a local attraction $-|U|$ between charge fluctuations and we restrict to hopping between nearest neighbor sites $\mathbf{R}_i$, $\mathbf{R}_j$ indicated by $\langle ij\rangle$. For the local potential V_i we consider a checkerboard geometry with alternating 4×4 plaquettes within which V_i varies between the values $V_i = 0$ and $V_i = -V_0$. Eq. (1) is solved via a standard BCS mean-field decoupling, see Supplementary Section I for details. Charge density and order parameter are enhanced on the plaquettes with $V_i = -V_0$ (Fig. 1b and d) and the resulting minibands display a flat character for sizeable V_0, Fig. 1c. The corresponding increased density of states induces a substantial enhancement of T_c, in particular at weak coupling, Fig. 2. In fact, for flat bands $T_c \sim |U|$ [25–28] while for dispersive bands the standard BCS relation $T_c \sim exp(-1/(N(0)|U|))$ applies, where $N(0)$ denotes the density of states at the Fermi level.

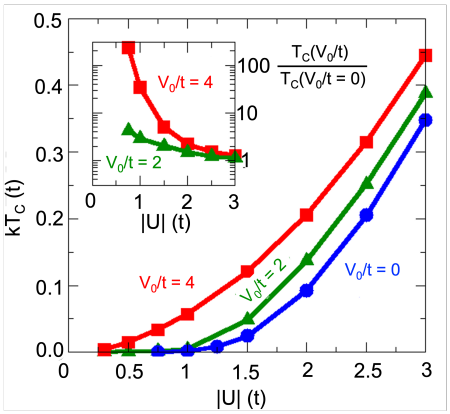


FIG. 2. **Critical temperature in the presence of a superpotential.** Comparison of T_c between homogeneous system ($V_0/t = 0$, blue) and in the presence of a superpotential with $V_0/t = 2$ (green) and $V_0/t = 4$ (red). Inset: Ratio between T_c with a finite superpotential and T_c for the homogeneous system. The solid red line in (e) is a fit to $T_c/T_c^{hom} = \alpha|U|e^{\beta t/|U|}$ with $\alpha = 0.0436$ and $\beta = 6.663$ as described in the text. Charge concentration: $p = 0.5$.

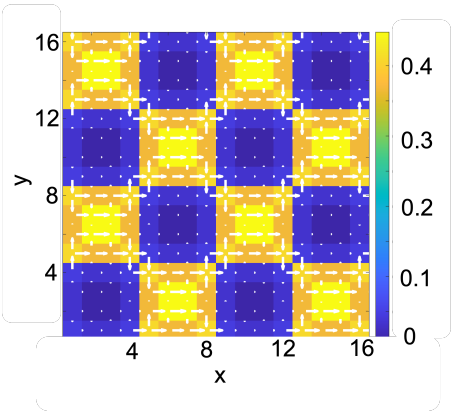


FIG. 3. **Current flow through the periodically modulated superconductor.** Illustration of the gauge invariant SC current distribution (white arrows) for a vector potential applied along the x-direction. The local gaps are shown as colored background. $U/t = 2$, $V_0/t = 4$, Charge concentration $n_{el} = 0.5$.

SUPERFLUID STIFFNESS

The superfluid stiffness D_s along a given direction α is calculated from the current correlation function $\chi_{jj}^{\alpha\alpha}$ [30]

$$D_s = -\langle T_\alpha \rangle - Re\chi_{jj}^{\alpha\alpha} \tag{2}$$

defined in the momentum limit $q_\parallel = 0, q_\perp \to 0, \omega = 0$ corresponding to the Meissner effect. It is composed of a diamagnetic part, in the present model equivalent to the negative kinetic energy $-\langle T_\alpha \rangle$ (that for parabolic dispersions equals the conventional n_s/m), and a paramagnetic term, which arises in inhomogeneous systems. Within our model this term contributes due to the presence of the superpotential scattering. Here we need to point out that contrary to conventional flat band systems we start from a model which has a finite kinetic energy. The multiband structure arises from the folding of the original band and splitting of the minibands due to the superpotential. Thus, even if the kinetic energy is reduced by the superpotential, it generally will remain finite, even if the miniband which crosses E_F becomes completely flat.

We also explore a parameter regime, where the interaction $|U|$ becomes larger than the hopping t. In this regime one cannot neglect the contribution of phase and charge fluctuations to the superfluid stiffness. These fluctuations take into account the phase relaxation of the SC order parameter in response to the applied vector potential and renormalize the stiffness for the inhomogeneous system [29]. Formally, this implies that the BCS current correlations have to be dressed by collective charge and order parameter fluctuations, cf. Supplementary Section IV. The total stiffness $D_s = D_s^{BCS} + D_s^{RPA}$ is composed of a BCS and a fluctuation contribution which we compute in the random phase approximation (RPA) [29]. This also ensures gauge invariance so that the SC currents are conserved at each node of the lattice, as shown in Fig. 3. One observes, that currents are dominant on the plaquettes with large SC order parameter and connect these plaquettes diagonally via currents along the y-direction. As shown in Supplementary Figure 2, within the BCS approximation instead one finds violation of charge conservation.

Fig. 4 shows the interaction dependence of D_s for $V_0/t = 4$ in comparison with the homogeneous case ($V_0/t = 0$) (blue line) within the BCS (light red line) and BCS+RPA approach (red full line), respectively. In the limit $|U|/t \to 0$, D_s approaches the Drude weight D_c, defined similarly to Eq. (2) but in the limit $\mathbf{q} = 0, \omega \to 0$ [30]. At $U/t = 0$ the stiffness $D_s = 0$ both for homogeneous and non-homogeneous systems.

For the homogeneous system one observes a slight reduction of the stiffness with increasing attractive interaction. Since in this case D_s is only due to the diamagnetic part, the behavior of the stiffness is solely determined by the increase of the kinetic energy (i.e. becoming less negative) with increasing order parameter which is the usual behavior for a BCS superconductor [31]. Upon increasing the superpotential V_0 the overall stiffness gets suppressed with respect to the homogeneous case due to the increasing paramagnetic contribution. In particular, we find that for $V_0/t = 4$ and $|U|/t < 0.5$ the stiffness almost vanishes ($D_s \approx 0$) which also holds for the charge stiffness ($D_c \approx 0$). For smaller values of V_0/t one still finds a finite stiffness in the limit $|U|/t \to 0$, see Supplementary Figure 3, while the enhancement of T_c is much less pronounced, see Fig. 2 (green curve). In case $V_0/t = 4$

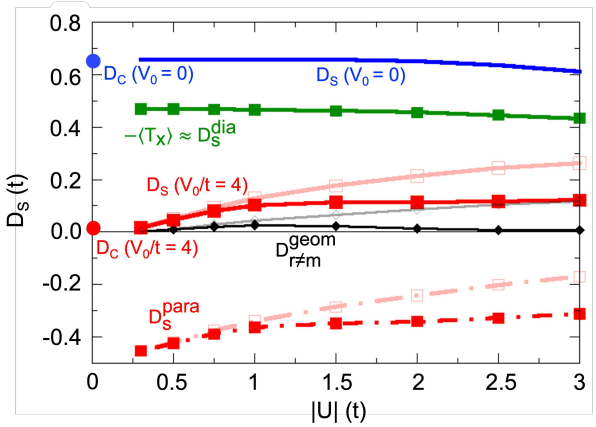


FIG. 4. **Impact of superpotential and gauge invariance on the superfluid stiffness.** Interaction dependence of the stiffness $D_{s,tot}$for superpotential values $V_0/t = 0$ (blue) and $V_0/t = 4$ (red, squares) separated into the diamganetic (mostly intraband) (D_s^{dia}) and paramagnetic (mostly interband) (D_s^{para}) contribution. Also shown is the geometric contribution for $r \neq m$ (black) which positively contributes to the stiffness. Lines in the foreground (full symbols) and in the background (open symbols) refer to the RPA (BCS) result, respectively. For $|U|/t = 0$ the charge stiffness D_c is shown by full circles while D_s vanishes in this limit. charge concentration: $p = 0.5$.

it is therefore remarkable that upon increasing the interaction the stiffness partially recovers and for $|U|/t = 3$ approaches a value of $D_s/t \approx 0.1$ (red full line) which is almost 17% of the value for the homogeneous system (blue line) so that πD_s is of the order of kT_c, cf. Fig. 2. Note also that the inclusion of phase relaxation via the BCS+RPA approach induces a significant reduction of the paramagnetic contribution to the stiffness from its BCS value (light red curve) for $|U|/t \gtrsim 1$. While the interaction dependence of D_s for $V_0/t = 4$ mimics the behavior one would expect from the geometric contribution in a flat band SC [11, 13], here the recovery of D_s is based on a different mechanism that, however, also includes a positive geometrical contribution. First, let us note that the kinetic term $-\langle T_\alpha \rangle$ (green line) stays finite due to the contribution of all occupied minibands as explained before. Second, the negative paramagnetic contribution (dashed-dotted line), which for $V_0/t = 4$ compensates the diamagnetic one at small $|U|/t$, becomes less negative upon increasing the attractive interaction. This can be understood based on the transfer of low energy spectral weight of the optical conductivity to its $\omega = 0$ pole with increasing SC gap as it is found in diffusive systems, see Supplementary Section VII. Nevertheless, we will show in the following that a certain geometric contribution is involved in this transfer of spectral weight.

This analysis is based on separation of the stiffness in a conventional (intraband) and a geometric (interband) contribution. The latter depends on the (real part of the) quantum metric tensor $g^{mn}_{\alpha\beta} = \langle n|\partial k_\alpha|m\rangle\langle m|\partial k_\beta|n\rangle$ [13] which is associated with the interband matrix elements of the current operator. The geometric contribution therefore manifests as a superconductivity induced spectral weight transfer in the optical conductivity of a multiband system, cf. Supplementary Section VI, and constitutes the dominating contribution to the stiffness in the conventional flat band limit.

We therefore rewrite the stiffness in the diagonal basis, cf. [12] which for the BCS contribution reads

$$D_s^{BCS} = -\frac{1}{N}\sum_{\substack{k,r,t,n,m \\ p_<,p_>}}{}' \Big\{\tau^\alpha_{r,t}(k,p_<,p_>)\delta_{rn}\delta_{tm} + 2\frac{C^\alpha_{r,t}(k,p_<,p_>)C^{\alpha,*}_{m,n}(k,p_<,p_>)}{\Omega_{p_>}+\Omega_{p_<}}\Big\} \quad (3)$$

where the indices r, t, n, m label the (normal state) miniband, and $p_{<(>)}$ refer to the quantum states in the SC state with energies $\Omega_{p_{<(>)}}$. τ^x is the diamagnetic contribution to the stiffness, expressed within these basis states, and C^α refer to the matrix elements of the current operator explicitely given in Supplementary Section III. The RPA-contribution can be cast into a similar form

$$D_s^{RPA} = \frac{1}{N}\sum_{\substack{k,r,t,n,m \\ p_<,p_>,p'_<,p'_>}}{}' C^\alpha_{r,t}(k,p_<,p_>) \times \Lambda^{RPA}(k,p_<,p_>,p'_<,p'_>)C^{\alpha,(*)}_{m,n}(k,p'_<,p'_>) \quad (4)$$

and the RPA kernel Λ^{RPA} is given in Supplementary Section IV. The conventional (intraband) contribution D^{intra} is obtained from Eqs. (3,4) by restricting the summation to $r = t$ and $n = m$ whereas the geometric contribution D^{inter} contains all the interband processes with $r \neq t$ and $n \neq m$.

We further separate the stiffness into intra-, inter- and mixed band contributions:

$$D_s \equiv \sum_{r,m}\mathcal{D}_{r,m} \equiv \sum_{r,t,n,m}\mathcal{D}_{r,t,n,m} \quad (5)$$

$$\mathcal{D}_{r,m} = \mathcal{D}^{intra}_{r,r,m,m} + \sum_{t\neq r,n\neq m}\mathcal{D}^{inter}_{r,t,n,m} + \sum_{n\neq m}\mathcal{D}^{mixed(1)}_{r,r,n,m} + \sum_{t\neq r}\mathcal{D}^{mixed(2)}_{r,t,m,m}. \quad (6)$$

The latter correspond to processes where one of the two current matrix elements $C^x_{r,t}$ in Eqs. (3,4) describes intra- and the other one interband scattering. It turns out that for present parameters the mixed contributions are smaller by a factor $\sim 10^{-2}$ than $\mathcal{D}^{intra/inter}$ and therefore will be neglected in the following discussion.

Fig. 5a shows $\mathcal{D}^{intra}_{r,r,m,m}$ where the diagonal elements $r = m$ are dominated by the (negative) kinetic energy contribution of band r. For the considered doping $p = 0.5$ the lowest (occupied) 8 bands contribute to the kinetic energy in the normal state. Due to particle-hole mixing

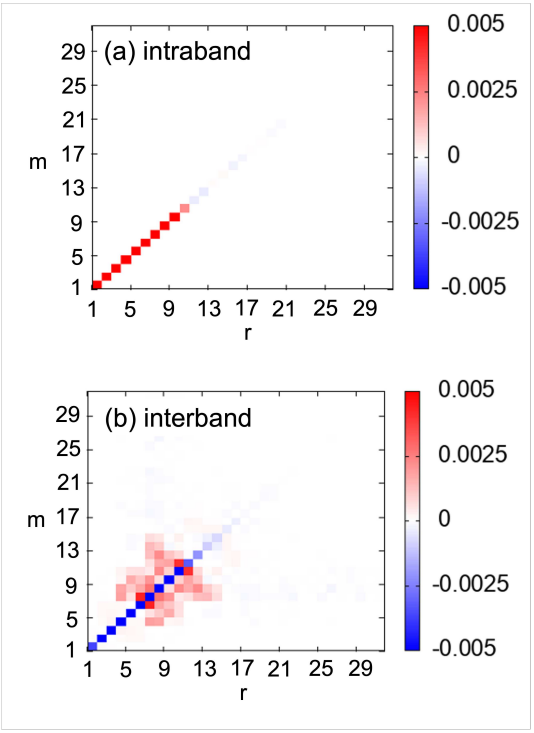


FIG. 5. **Intra- and interband contributions to the superfluid stiffness.** Color surface plot of $\mathcal{D}_{r,m}$, see Eq. (5), divided into intraband (a) and interband (b) contributions. charge concentration $p = 0.5$; $|U|/t = 2$.

there is also a contribution from bands above the chemical potential in the presence of SC. The sum over all contributions in Fig. 5a is very close to the diamagnetic term, i.e. the total kinetic energy. On the other hand, the sum over the interband (i.e. geometric) contributions $D^{geom}_{r,m} = \sum_{t,n} \mathcal{D}^{inter}_{r\neq t,n\neq m}$ in Fig. 5b is always negative and is close to the (negative) paramagnetic term. It can be seen that this is dominated by diagonal elements $\mathcal{D}^{geom}_{m,m}$ which means that in Eq. (6) the two current matrix elements describe scattering processes which involve a common band $r = m$. Interestingly, we also find a positive interband term $D^{geom}_{r\neq m}$ (cf. black curve in Fig. 4) which in conventional flat band systems would constitute the dominating contribution to the stiffness. It scales with the interaction and represents a significant fraction of $20\% - 30\%$ of the total stiffness in weak coupling while its contribution becomes suppressed due to phase relaxation for $|U|/t \gg 1$.

CONSIDERATION OF DISORDER

Within our 'mean-field' BCS approach the critical temperature kT_c can be associated with the pairing energy scale whereas πD_s sets the scale for phase coherence. In the weak-coupling BCS limit one therefore always finds $\pi D_s/kT_c \gg 1$ since phase coherence is already established when Cooper pairs start to form. In the low-disorder regime where the mean free path is much longer than the inverse Fermi wave vector, $k_F l \gg 1$, the stiffness slightly decreases due to the paramagnetic contribution while Anderson's theorem [32] for the pairing of time-reversed exact eigenstates leaves T_c unchanged. The situation changes when $k_F l \approx 1$ and Cooper pairs can start to form above the temperature where phase coherence sets in, cf. e.g. Ref. [33]. In this regime the stiffness becomes comparable with kT_c eventually leading to a superconductor-insulator transition ($D_s = kT_c = 0$) when disorder exceeds a critical value as e.g. observed in TiN, InO_x and NbN films [34–36].

Charge carriers in flat band systems are very susceptible toward localization so that the stiffness, which depends inversely on the mass, also sensitively depends on the amount of disorder when the strength of the superpotential becomes sizeable.

In order to investigate the influence of disorder we add to the hamiltonian Eq. (1) an impurity potential $V = \sum_{n\sigma} I_n n_{n\sigma}$ where the I_n are drawn from a flat distribution with $-I_0 \leq I_n \leq I_0$. In this way disorder is treated exactly, cf. Supplementary Section II, and we evaluate the resulting stiffness by averaging the current correlations over $10 - 20$ disorder configurations.

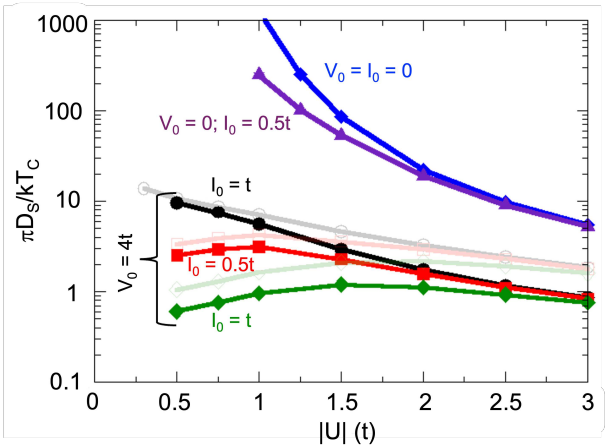


FIG. 6. **Ratio between the superfluid stiffness and T_c.** Blue and violet curves are for the system without superpotential and impurity potentials $I_0/t = 0.$ and $I_0/t = 0.5$, respectively. In the presence of a superpotential ($V_0/t = 4$, patch size 4×4) the results are shown for impurity strength $I_0/t = 0$ (black), $I_0/t = 0.5$ (red), $I_0/t = 1$ (green). Lines in the foreground (full symbols) and background (open symbols) refer to the RPA (BCS) result, respectively. In case of $V_0 = I_0 = 0$ RPA and BCS result are identical, whereas for $V_0 = 0$, $I_0 = 0.5t$ the difference is within the size of the symbols. Charge density $n_{el} = 0.5$.

We consider two values for the impurity potential $I_0/t = 0.5$ and $I_0/t = 1$ which, upon solving the temperature dependent gap equation, have only minor influence on T_c. The relaxation time is obtained by fitting

$\sigma(\omega)$ to the Drude formula, see Supplementary Section V and k_F is determined from the average of the Fermi momentum over the Fermi surface of the homogeneous system. For $I_0/t = 0.5$ this yields a value of $k_F l \approx 40$ and a mean free path of $l \approx 23$ in units of the lattice spacing which is larger than the superlattice periodicity. In case of $I_0/t = 1$ one finds $k_F l \approx 10$ and $l \approx 6$ which is of the order of the superlattice periodicity (we recall that for the 4×4 plaquette structure the translation vectors are $\vec{a}_1 = (8, 0)$ and $\vec{a}_2 = (4, 4)$ in units of the lattice constant).

Fig. 6 compares $\pi D_s/(kT_c)$ for systems with and without superpotential and impurities. In the clean and homogeneous case ($V_0/t = I_0/t = 0$, blue) the typical BCS behavior is recovered where in the weak coupling limit the stiffness exceeds the pairing scale kT_c by several orders of magnitude and the ratio $\pi D_s/(kT_c)$ decreases towards stronger coupling. In fact, since in the homogeneous system the stiffness only weakly depends on $|U|$, the behavior can be understood from the weak-coupling BCS result $T_c \sim e^{-1/(|U|N_0)}$ where N_0 denotes the density of states. This yields $ln(D_s/T_c) \sim 1/|U|$ which is exactly the behavior shown in Fig. 6 for the homogeneous system. For a moderate impurity strength ($V_0/t = 0; I_0/t = 0.5$, violet) the stiffness of the homogeneous system is reduced in particular at weak coupling while for larger interaction it approaches the value of the clean case.

In the presence of a superpotential but without impurities ($V_0/t = 4; I_0/t = 0$, black) the ratio $\pi D_s/kT_c$ is substantially smaller than for the homogeneous system, in particular at weak coupling. On the one hand, this is due to the smaller stiffness in this regime (cf. Fig. 4) but more relevant is the exponentially larger T_c, cf. inset to Fig. 2. While for the clean superpotential $\pi D_s/kT_c \approx 10$, one finds a further reduction of this value at weak coupling $|U|/t = 0.5$ due to the addition of impurities. We also observe that $\pi D_s/kT_c$ goes through a maximum upon decreasing the interaction and for impurity strength $I_0/t = 1$ (green) it approaches $\pi D_s/kT_c \approx 1$ for $|U|/t = 0.5$. Thus, this limit is obtained when the mean free path becomes of the order of the superpotential periodicity.

DISCUSSION

The periodic superpotential can substantially enhance the critical temperature while preserving a sizeable stiffness that scales with the interaction strength. Unlike conventional flat-band systems, where filled bands do not contribute to the kinetic energy and a finite stiffness arises solely from the positive quantum geometric term, our periodically modulated system retains contributions from all minibands below the chemical potential. As a result, even when the top band is flat, a finite diamagnetic response persists. The interband term is overall negative but includes a positive quantum geometric component. Thus, superlattice engineering offers a promising route to enhance Tc, as the system effectively inherits the stiffness of the homogeneous case. It is interesting that recent theoretical work succeeded to predict the topological properties of materials subject to a superlattice potential [37]. In particular, the periodic patterning of a 2D electron gas [38] reveals a non-zero local Berry phase for antisymmetric triangular superpotentials. This geometry therefore could further sustain the superfluid stiffness because of topology. Consideration of such structures will be considered in future studies within the Usadel equations which allow for the treatment of superpotentials which are incommensurate with the host lattice.

It should be noted that the model here differs from previous work which studied the competition between charge-density wave and SC order parameters [39, 40]. Here instead, we are not considering competing instabilities since the superpotential is imposed on the system via external periodic gating [41] or nanostructuring [42] so that the Fermi level can in principle be tuned into one of the flat bands. This leads to an enhancement of T_c with respect to the homogeneous system which at weak coupling can reach one or two orders of magnitude, cf. inset to Fig. 2. It is to be expected that the influence of phase fluctuations will affect this amplification if the mean free path in the disordered system is of the same order of magnitude as the periodicity of the superlattice which corresponds to the limit $\pi D_s/kT_c \approx 1$. For strongly disordered NbN films [33] it has been shown that the transition temperature toward a coherent SC state is reduced by a factor ~ 3 when this ratio decreases from $\pi D_s/kT_c \approx 5$ to $\pi D_s/kT_c \approx 1$ so that our results are still compatible with a significant enhancement of T_c.

Yet, there are still a few hurdles to overcome in order to realize such a system with increased transition temperature and robust stiffness. First, secondary instabilities such as magnetism may occur when the Fermi level is located in one of the flat bands.

The concomitant opening of additional gaps will then compete with the T_c enhancement although the system may remain in a state with sizeable stiffness. Second, as we have seen the system should be sufficiently clean so that the stiffness still dominates the energy scale of the transition temperature. In principle, this requirement should be achievable with $LaAlO_3/SrTiO_3$ interfaces where tunable superconductivity has been observed below 0.3 K [43]. Here one can reach mobilities as high as 10.000 cm^2/Vs, corresponding to a mean free path of about 100 nm [44]. This is well beyond the 40 nm pitch limit of standard e-beam lithography which defines the possible lower bound periodicity of the metal gate superpotential [45].

To conclude, this work demonstrates that applying a superpotential can provide a solid foundation for enhancing superconductivity, even in single-band systems. It

thereby paves the way for engineering diverse superpotential architectures as a powerful strategy to design and control superconductivity.

The authors acknowledge support from the Swedish Research Council (VR), under the Projects 2018-04658 (F.L.) and 2020-05184 (T.B.), and by the Deutsche Forschungsgemeinschaft, under SE 806/20-1 (G.S.).

[1] R. Bistritzer and A. H. MacDonald, Moiré bands in twisted double layer graphene, Proc. Natl. Acad. Sci. USA **108**(30), 12233 (2011).
[2] J. M. B. Lopes dos Santos, N. M. R. Peres, and A. H. Castro Neto, Graphene Bilayer with a Twist: Electronic Structure. Phys. Rev. Lett. **99**, 256802 (2007).
[3] Yuan Cao, Valla Fatemi, Shiang Fang, Kenji Watanabe, Takashi Taniguchi, Efthimios Kaxiras, and Pablo Jarillo-Herrero, Unconventional superconductivity in magic-angle graphene superlattices. Nature **556**, 43 (2018).
[4] Yuan Cao, Valla Fatemi, Ahmet Demir, Shiang Fang, Spencer L. Tomarken, Jason Y Luo, Javier D. Sanchez-Yamagishi, Kenji Watanabe, Takashi Taniguchi, Efthimios Kaxiras, Ray C. Ashoori, and Pablo Jarillo-Herrero, Correlated insulator behaviour at half-filling in magic-angle graphene superlattices, Nature **556**, 80 (2018).
[5] Xiaobo Lu, Petr Stepanov, Wei Yang, Ming Xie, Mohammed Ali Aamir, Ipsita Das, Carles Urgell, Kenji Watanabe, Takashi Taniguchi, Guangyu Zhang, Adrian Bachtold, Allan H. MacDonald, and Dmitri K. Efetov, Superconductors, orbital magnets and correlated states in magic-angle bilayer graphene. Nature **574**, 653 (2019).
[6] A.L. Sharpe1, E.J. Fox, A.W. Barnard, J. Finney, K. Watanabe, T. Taniguchi, M.A. Kastner, D. Goldhaber-Gordon, Emergent ferromagnetism near three-quarters filling in twisted bilayer graphene. Science **365**, 605 (2019).
[7] A. Kerelsky, L.J. McGilly, D.M. Kennes, L. Xian, M. Yankowitz, S. Chen, K. Watanabe, T. Taniguchi, J. Hone, C. Dean, A. Rubio, and A.N. Pasupathy, Maximized electron interactions at the magic angle in twisted bilayer graphene. Nature **572**, 95 (2019).
[8] Matthew Yankowitz, Shaowen Chen, Hryhoriy Polshyn, Yuxuan Zhang, K. Watanabe, T. Taniguchi, David Graf, Andrea F. Young, Cory R. Dean, Tuning superconductivity in twisted bilayer graphene. Science **363**, 1059 (2019).
[9] L. Balents, C.R. Dean, D.K. Efetov, and A.F. Young, Superconductivity and strong correlations in moiré flat bands. Nat. Phys. **16**, 725–733 (2020).
[10] S. Peotta and P. Törmä, Superfluidity in topologically nontrivial flat bands, Nat. Commun. **6**, 8944 (2015).
[11] A. Julku, S. Peotta, T. I. Vanhala, D. H. Kim, and P. Törmä, Geometric Origin of Superfluidity in the Lieb-Lattice Flat Band, Phys. Rev. Lett. **117**, 045303 (2016).
[12] Long Liang, Tuomas I. Vanhala, Sebastiano Peotta, Topi Siro, Ari Harju, and P. Törmä, Phys. Rev. B **95**, 024515 (2017).
[13] Junyeong Ahn and Naoto Nagaosa, Superconductivity-induced spectral weight transfer due to quantum geometry. Phys. Rev. B **104**, L100501 (2021).
[14] P. Törmä, S. Peotta, and B. A. Bernevig, Superconductivity, superfluidity and quantum geometry in twisted multilayer systems. Nature Review Physics **4**, 528 (2022).
[15] P. Törmä, Essay: Where Can Quantum Geometry Lead Us? Phys. Rev. Lett. **131**, 240001 (2023).
[16] J. Yu, B. A. Bernevig, R. Queiroz, E. Rossi, P. Törmä, and B.-J. Yang, Quantum geometry in quantum materials. npj Quantum Materials **10**, 101 (2025).
[17] A. Gao, N. Nagaosa, N. Ni, and S.-Y. Xu, Quantum Geometry Phenomena in Condensed Matter Systems. arXiv:2508.00469.
[18] N. Verma, P. J. W. Moll, T. Holder, and R. Queiroz, Quantum Geometry: Revisiting electronic scales in quantum matter. arXiv:2504.07173.
[19] S. Peotta, K.-E. Huhtinen, and P. Törmä, Quantum geometry in superfluidity and superconductivity. Proceedings of the International School of Physics "Enrico Fermi", Course 211 "Quantum Mixtures with Ultra-Cold Atoms. p. 373 (2025).
[20] G. Shavit and Y. Oreg, Quantum Geometry and Stabilization of Fractional Chern Insulators Far from the Ideal Limit. Phys. Rev. Lett **133**, 156504 (2024).
[21] G. Jiang and Y. Barlas, Geometric superfluid weight of composite bands in multiorbital superconductors. Phys. Rev. B **109**, 214518 (2024).
[22] Y.-J. Hu and W. Huang, Quantum geometric superfluid weight in multiband superconductors: A microscopic interpretation. phys. Rev. B **111**, 134511 (2025).
[23] G. Sala, M. T. Mercaldo, K. Domi, S. Gariglio, M. Cuoco, C. Ortix, and A. D. Caviglia, The quantum metric of electrons with spin-momentum locking. Science **389**, 822 (2025).
[24] J. Yu, C. J. Ciccarino, I. Errea, P. Narang, R. Bianco, and B. A. Bernevig, Non-trivial quantum geometry and the strength of electron–phonon coupling. Nature Physics **20**, 1262 (2024).
[25] V. A. Khodel and V. R. Shaginyan, Superfluidity in system with fermion condensate. JETP Lett. **51**, 553 (1990).
[26] V.A. Khodel, V.R. Shaginyan, and V.V. Khodel, New approach in the microscopic Fermi systems theory. Physics Reports **249**, 1 (1994).
[27] N.B. Kopnin, T.T. Heikkilä, and G.E. Volovik, High-Temperature Surface Superconductivity in Topological Flat-Band Systems, Phys. Rev. B **83**, 1 (2011).
[28] G.E. Volovik, Graphite, Graphene, and the Flat Band Superconductivity. Jetp Lett. **107**, 516–517 (2018).
[29] G. Seibold, L. Benfatto, C. Castellani, and J. Lorenzana, Superfluid Density and Phase Relaxation in Superconductors with Strong Disorder. Phys. Rev. Lett. **108**, 207004 (2012).
[30] D. J. Scalapino, S. R. White, and S. Zhang, Insulator, metal, or superconductor: The criteria. Phys. Rev. B **47**, 7995 (1993).
[31] J. Bardeen, L. N. Cooper, and J. R. Schrieffer, Theory of Superconductivity. Physical Review **108**, 1175 (1957).
[32] P. W. Anderson, Theory of dirty superconductors. J. Phys. Chem. Solids **11**, 26 (1959).
[33] M. Mondal, A. Kamlapure, S.C. Ganguli, J. Jesudasan, V. Bagwe1, L. Benfatto, and P. Raychaudhuri, Enhancement of the finite-frequency superfluid response in the pseudogap regime of strongly disordered superconducting films. Sci Rep **3**, 1357 (2013). https://doi.org/10.1038/srep01357.
[34] B. Sacépé, T. Dubouchet, C. Chapelier, M. Sanquer, M.

Ovadia, D. Shahar, M. Feigel'Man, L. Ioffe, Localization of preformed Cooper pairs in disordered superconductors. Nature Physics **7**, 239 (2011).

[35] B. Sacépé, C. Chapelier, T. Baturina, V.M. Vinokur, M.R. Baklanov, and M. Sanquer, Pseudogap in a thin film of a conventional superconductor. Nat Commun. **1**, 140 (2010). https://doi.org/10.1038/ncomms1140

[36] M. Mondal, A. Kamlapure, M. Chand, G. Saraswat, S. Kumar, J. Jesudasan, L. Benfatto, V. Tripathi, and P. Raychaudhuri, Phase fluctuations in a strongly disordered s-wave NbN superconductor close to the metal-insulator transition. Phys. Rev. Lett. **106**, 047001 (2011).

[37] V. Crépel and J. Cano, Efficient Prediction of Superlattice and Anomalous Miniband Topology from Quantum Geometry. Physical Review X **15**, 011004 (2025).

[38] P.A. Pantaleón, Z. Zhan , S.E. Morales, and G.G. Naumis, Designing flat bands and pseudo-Landau levels in GaAs with patterned gates. Phys. Rev. B**111**, 245303 (2025).

[39] C. A. Balseiro and L. M. Falicov, Superconductivity and charge-density waves, Phys. Rev. B **20**, 4457(1979).

[40] A. M. Gabovich, A. I. Voitenko, and M. Ausloos, Charge- and spin-density waves in existing superconductors: competition between Cooper pairing and Peierls or excitonic instabilities. Physics Reports **367**, 583 (2002).

[41] D.Q. Wang, Z. Krix, O.A. Tkachenko, V.A. Tkachenko, C. Chen, I. Farrera, D.A. Ritchie, O.P. Sushkov, A.R. Hamilton, and O. Klochan, Tuning the bandstructure of electrons in a two-dimensional artificial electrostatic crystal in GaAs quantum wells. arXiv:2402.12769v1.

[42] E. Wahlberg, R. Arpaia, D. Chakraborty, A. Kalaboukhov, D. Vignolles, C. Proust, A. M. Black-Schaffer, G. Seibold, T. Bauch, and F. Lombardi, Boosting superconductivity: how nanofaceted surfaces transform the ground state of ultrathin $YBa_2Cu_3O_{7-\delta}$ thin films. Accepted in Nat. Commun. arXiv:2502.03986.

[43] J. Biscaras, N. Bergeal, S. Hurand, C. Grossetête, A. Rastogi, R. C. Budhani, D. LeBoeuf, C. Proust, and J. Lesueur, Two-Dimensional Superconducting Phase in $LaTiO_3/SrTiO_3$ Heterostructures Induced by High-Mobility Carrier Doping, Phys. Rev. Lett. **108**, 247004 (2012).

[44] G. Singh, R. Guzman, G. Saïz, W. Zhou, J. Gazquez, F. Masoudinia, D. Winkler, T. Claeson, J. Fraxedas, N. Bergeal, G. Herranz, and A. Kalaboukhov, Stoichiometric control of electron mobility and 2D superconductivity at LaAlO3-SrTiO3 interfaces. Commun Phys. **7**, 149 (2024).

[45] C. Forsythe, X. Zhou, K. Watanabe, T. Taniguchi, A. Pasupathy, P. Moon, M. Koshino, P. Kim, C. R. Dean, Band structure engineering of 2D materials using patterned dielectric superlattices. Nature Nanotechnology **13**, 566 (2018).

Supplementary Files

This is a list of supplementary files associated with this preprint. Click to download.

- supplementary.pdf